

Non-Local Simulation of the Formation of Neoclassical Ambipolar Electric Field in Non-Axisymmetric Configurations

Shinsuke SATAKE, Masao OKAMOTO, Noriyoshi NAKAJIMA,
Hideo SUGAMA and Masayuki YOKOYAMA

National Institute for Fusion Science, Toki 509-5292, Japan

(Received 25 November 2004 / Accepted 28 November 2005)

Neoclassical transport simulation code (FORTEC-3D) applicable to non-axisymmetric configurations is developed. A new hybrid simulation model in which ion transport is solved by using the δf Monte-Carlo method including the finite-orbit-width effects, while electron transport is solved by a reduced ripple-averaged kinetic equation, is adopted. This model makes it possible to simulate the dynamism of non-local transport phenomena with a self-consistently developing radial electric field within an allowable computation time. Time evolution of a radial electric field in LHD plasma is simulated in the full volume of the confinement region, and the finite-orbit-width effect of neoclassical transport is found to make the negative ambipolar electric field larger than that predicted by local transport theory.

© 2006 The Japan Society of Plasma Science and Nuclear Fusion Research

Keywords: neoclassical transport, ambipolar electric field, finite-orbit-width effect

DOI: 10.1585/pfr.1.002

1. Introduction

Neoclassical transport theory has been successfully established under the assumption of the local transport model (small-orbit-width limit) and in a quasi-steady state. However, these assumptions cannot be used to investigate those issues which have been recently attracting much interests, such as the finite-orbit-width (FOW) effects when the typical orbit width in the radial direction is comparable to the background gradient scale, the geodesic acoustic mode (GAM) of the electric field and its Landau damping mechanism [1], and the evolution of the ambipolar radial electric field E_r . Though the net radial transport level observed in experiments is usually dominated by anomalous transport, the self-induced electric field profile can be explained by the neoclassical transport theory. We have shown [2] by Monte-Carlo simulation using the δf method [3, 4] that in tokamak cases a steep E_r profile can be formed if there exists a steep density gradient. Such a sheared E_r profile is considered to reduce both the neoclassical transport level by the orbit-squeezing effect [5] and microscopic turbulence by the $E \times B$ shearing effect. In non-axisymmetric cases, steep shear in the E_r profile can also be formed if the ambipolar condition has multiple solutions [6]. Since the neoclassical fluxes in helical plasma strongly depend on E_r , the determination of a radial electric field in the existence of multiple ambipolar roots is a key issue to evaluate the transport level in helical plasma.

The transition and bifurcation phenomena of E_r in helical systems have usually been studied by using an analytic model for neoclassical transport [7, 8], for example

in [6, 9]. These previous studies have focused on relatively slow-time scale phenomena, that is, the transport time scale in which background profile of density and temperature change. We are interested in shorter time-scale phenomena comparable to transit time $\tau_{tr} \sim qR/v_{th}$ to ion collision time τ_i where the background density and temperature profiles can be considered unchanged. However, the analytic model of neoclassical transport lacks the following physical mechanisms: 1) GAM oscillation and polarization drift motion associated with rapid time evolution of radial electric field, 2) non-local drift motion of transit particle orbits in non-axisymmetric configuration and its contribution to neoclassical transport, 3) direct orbit loss at the plasma boundary, and 4) rigorous treatment of the Coulomb collision. To simulate the dynamic transport process and the formation of the ambipolar electric field including non-local effects in non-axisymmetric configurations, we have been developing the δf code FORTEC-3D to be applicable to general 3-dimensional configurations. The formulation is explained in Sec. 2. In FORTEC-3D, neoclassical ion transport is solved by the δf method while electron one is obtained from a ripple-averaged kinetic equation solver GSRAKE [10, 11], and the time evolution of E_r is solved self-consistently in the simulation. The adoption of this hybrid simulation model enables us to simulate neoclassical transport including the FOW effect of ions within an allowable computation time. For a demonstration of the new simulation model, in Sec. 3 we show the global simulation results of the time evolution of the radial electric field in LHD plasmas [12]. The formation of the ambipolar E_r profile in the presence of multiple

author's e-mail: satake@nifs.ac.jp

roots for the ambipolar condition is successfully simulated, and it is found that the FOW effect changes the ambipolar electric field profile from that obtained by conventional local transport analysis.

2. Simulation Model

In the δf method, time development of the perturbation of plasma distribution function from the local Maxwellian $\delta f = f - f_M$ is solved according to the drift-kinetic equation

$$\begin{aligned} \frac{D\delta f}{Dt} &\equiv \frac{\partial \delta f}{\partial t} + (\mathbf{v}_{\parallel} + \mathbf{v}_d) \cdot \nabla \delta f - C_{\text{tp}}(\delta f) \\ &= -\mathbf{v}_d \cdot \nabla f_M + \mathcal{P}f_M, \end{aligned} \quad (1)$$

where C_{tp} and \mathcal{P} are test-particle and field-particle parts of a linearized collision operator, $\mathbf{v}_{\parallel} = \mathbf{v} \cdot \mathbf{B}/B$, and \mathbf{v}_d is the drift velocity of guiding center motion across the magnetic field line. The magnetic field is given in the Boozer coordinate system (ψ, θ, ζ) [13] as $\mathbf{B} = \nabla\psi \times \nabla\theta + \tau \nabla\zeta \times \nabla\psi$, where ψ is the toroidal flux, θ and ζ are poloidal and toroidal angles, and τ is the rotational transform divided by 2π , respectively. In our simulation, the magnetic field configuration is constructed from the VMEC code [14] which solves the MHD equilibrium state for a given pressure and plasma current profiles. The guiding center equations of motion in the Boozer coordinates are also described in [13]. The guiding center motion of simulation markers, whose distribution function is here expressed as g , is traced in 5-dimensional phase space $(\psi, \theta, \zeta, v_{\parallel}, v_{\perp})$. The test-particle collision operator C_{tp} is implemented numerically by random kicks of marker velocity in the $(v_{\parallel}, v_{\perp})$ space. $\mathcal{P}f_M$ is then defined so that the three constants in the exact Fokker-Planck collision operator, i.e., total particle number, moments, and energy, should really be conserved. The details of the collision operator used here is described in [3]. To solve eq. (1), two weights, w and p , are introduced which satisfy the relations $wg = \delta f$ and $pg = f_M$, respectively. Since the time evolution of marker distribution can be described by $Dg/Dt = 0$, where D/Dt means the total derivative along marker motion including stochastic motion by the effect of C_{tp} , these weights evolve according to

$$\frac{dw}{dt} = \frac{p}{f_M} [-\mathbf{v}_d \cdot \nabla + \mathcal{P}] f_M, \quad (2a)$$

$$\frac{dp}{dt} = \frac{p}{f_M} \mathbf{v}_d \cdot \nabla f_M. \quad (2b)$$

Note that the FOW effect is included from the $\mathbf{v}_d \cdot \nabla \delta f$ term in eq. (1), which is omitted in standard neoclassical theory.

Neoclassical particle and energy fluxes are evaluated by

$$\Gamma = \left\langle \int d^3v \psi \delta f \right\rangle, \quad (3a)$$

$$q = \left\langle \int d^3v \frac{1}{2} m v^2 \psi \delta f \right\rangle, \quad (3b)$$

where $\langle \dots \rangle$ means the flux-surface average. The time evolution of radial electric field $\mathbf{E} = -d\Phi/d\psi \nabla\psi = E_{\psi} \nabla\psi$ can

be described as follows

$$\epsilon_0 \left[\langle |\nabla\psi|^2 \rangle + \left\langle \frac{c^2}{v_A^2} |\nabla\psi|^2 \right\rangle \right] \frac{\partial E_{\psi}}{\partial t} = -e [z_i \Gamma_i - \Gamma_e], \quad (4)$$

where subscripts i and e describe particle species, and v_A is the Alfvén velocity. The term containing v_A appears because of the classical polarization drift proportional to $\partial \mathbf{E}/\partial t$. The neoclassical polarization drift, which can be explained by considering the drift of bounce-averaged position $\oint dt \dot{\psi}/\tau_b$ when E_{ψ} is time-dependent, is included in the evaluation of eq. (3) because we trace the marker orbit directly in the time-dependent field without any averaging operation in solving the equations of motion. Similarly, the orbit squeezing effect is also included in eq. (3) since the marker orbit is traced exactly including the radial excursion in a sheared E_{ψ} field.

In our previous study of tokamak plasmas, electron particle flux Γ_e has been neglected because of its smallness. In non-axisymmetric cases, however, Γ_e becomes comparable to Γ_i and is needed in order to simulate the time evolution of the ambipolar electric field in which $\Gamma_e(\psi, E_{\psi}) = z_i \Gamma_i(\psi, E_{\psi})$ is satisfied. The hybrid simulation model for evaluating Γ_e and Γ_i introduced in Sec. 1 is adopted since the FOW effect is expected to be important mainly on ions which have a wider radial orbit width than electrons. The details of the GSRAKE code used to evaluate Γ_e are found in the references [10, 11]. In brief, GSRAKE solves ripple-averaged (or so-called bounce-averaged) kinetic equation in helical systems. One advantage of GSRAKE over other analytic models is that it treats both ripple-trapped particles and non-localized (passing) particles on an equal footing in the formulation. It can be applicable to the whole long-mean-free-path regime ($v_{\text{eff}}/\tau_b \ll 1$) and a wide range of E_{ψ} . Therefore, it is suitable to make the table of $\Gamma_e(\psi, E_{\psi})$ in the entire simulation domain (ψ, E_{ψ}) where the collisionality and E_{ψ} may change to a large extent. The Γ_e -table is then referred to in each step in FORTEC-3D to evaluate eq. (4). The reliability of the result obtained by GSRAKE in the LHD configuration has been benchmarked in the above references.

Because a magnetic coordinate system is used, we have no information beyond the last closed flux surface (LCFS). The magnetic field spectrum is extrapolated to the outer region, and markers that spend some time steps out of the LCFS are killed and recycled inside the LCFS. This procedure corresponds to a orbit-loss mechanism at the boundary. Recycled marker weights should be determined so as not to bring any physical value such as particle density, momentum, and energy into the rebirth point. For the weight w , the new weight can most easily set as 0 for recycled markers. However, this causes a numerical noise because these recycled markers enhance the spread of weight field variance. In fact, the weight spread is essentially inevitable in the δf Monte-Carlo method [4] because two markers which have moved on different paths

in the phase space come up to the same point at the same time with bringing different weights. We have expanded the weight-averaging technique described in Ref. [4] for the determination of the new markers' weights as follows. (Though here we only show the procedure for weight w , it can also be applied in determining p .)

At first, consider an averaged weight field $W_{ij}(\mathbf{v})$ in a small bin (i, j) in the velocity space $(v_{\parallel}, v_{\perp})$. We assume that W_{ij} is given in the following form

$$W_{ij}(\mathbf{v}) = W_{ij}^{(0)} + W_{ij}^{(1)}v_{\parallel} + W_{ij}^{(2)}v^2. \quad (5)$$

Next, the weight for existing markers w_k and newly recycled ones w_l in the (i, j) bin are renewed toward $W_{ij}(\mathbf{v})$ with a damping rate γ ($0 < \gamma < 1$),

$$w_k^1 = \gamma W_{ij}(\mathbf{v}_k) + (1 - \gamma)w_k^0, \quad (6a)$$

$$w_l^1 = W_{ij}(\mathbf{v}_l), \quad (6b)$$

where overscripts 0 and 1 denote the old and new value, respectively. To prevent the sums of constants-of-motion in a bin from changing on recycling, the following relations must be satisfied.

$$\sum_k w_k^0 = \sum_k w_k^1 + \sum_l w_l^1, \quad (7a)$$

$$\sum_k w_k^0 v_{\parallel k} = \sum_k w_k^1 v_{\parallel k} + \sum_l w_l^1 v_{\parallel l}, \quad (7b)$$

$$\sum_k w_k^0 v_k^2 = \sum_k w_k^1 v_k^2 + \sum_l w_l^1 v_l^2. \quad (7c)$$

Combining eqs. (5)-(7), one obtains the following relation, which is inverted to determine $W_{ij}^{(0,1,2)}$,

$$\gamma \begin{pmatrix} \sum_k w_k^0 \\ \sum_k w_k^0 v_{\parallel k} \\ \sum_k w_k^0 v_k^2 \end{pmatrix} = \begin{pmatrix} \gamma k_{ij} + l_{ij} & \sum_{k,l} \gamma v_{\parallel k} + v_{\parallel l} & \sum_{k,l} \gamma v_k^2 + v_l^2 \\ \sum_{k,l} \gamma v_{\parallel k}^2 + v_{\parallel l}^2 & \sum_{k,l} \gamma v_{\parallel k} v_k^2 + v_{\parallel l} v_l^2 & \\ \sum_{k,l} \gamma v_k^4 + v_l^4 & & \end{pmatrix} \begin{pmatrix} W_{ij}^{(0)} \\ W_{ij}^{(1)} \\ W_{ij}^{(2)} \end{pmatrix}, \quad (8)$$

where the matrix is symmetric, and k_{ij} , l_{ij} are the numbers of existing and recycling markers in a bin, respectively. We have verified that the recycling procedure performed effectively without increasing the weight variance at the rebirth region for 6,000 computation time steps, which correspond to $t = 3.0\tau_i$. By introducing the recycling technique, it is possible to trace the time evolution of the radial electric field up to a few collision times which is required to simulate the transport phenomena until the distribution function δf reaches a quasi-steady state.

3. Transport Simulation in LHD Plasma

We have conducted transport simulation using FORTEC-3D in several configurations. The magnetic field configuration is constructed modeled on a LHD plasma in which the magnetic axis and magnetic field strength on it are $R_{ax} = 3.7$ m and $B_0 = 1.65$ T, respectively. The density and temperature profiles for ions and electrons are given by the following expression

$$\begin{Bmatrix} n_{i,e}(\rho) \\ T_{i,e}(\rho) \end{Bmatrix} = \begin{Bmatrix} n_{0i,e} \\ T_{0i,e} \end{Bmatrix} [\alpha_1 + (1 - \alpha_1) \exp(-\alpha_2 \rho^{\alpha_3})], \quad (9)$$

where $\rho = \sqrt{\psi/\psi_{edge}}$ is the normalized minor radius, and $(\alpha_1, \alpha_2, \alpha_3) = (-0.01, 3.0, 3.5)$ for density and $(0.05, 4.5, 2.0)$ for temperature. In the first case, we set $T_{0i} = T_{0e} = 1.0$ keV and $n_{0i} = n_{0e} = 2.0 \times 10^{18} m^{-3}$. The plasma collisionality is considered to be in the $1/\nu$ regime [16] in almost the entire plasma region. We have used $60 \times 20 \times 10$ meshes in the ψ , θ , and ζ -directions respectively, and 20×10 meshes in the velocity space $(v_{\parallel}, v_{\perp})$. The simulation domain is restricted to a one-helical pitch ($0 < \zeta < \pi/5$) and a cyclic boundary condition is set in the ζ -direction. Sixty-four million markers have been used in the simulation. Such a large number of markers are required to suppress the statistical noise in the long-duration simulation up to a few collision times. Though the simulation becomes heavy in the 3-dimensional cases, it takes only 10 hours to run up to $1.0\tau_i$ on the supercomputer system in NIFS owing to the high parallelization and vectorization efficiency of the code written in HPF (High Performance Fortran) [15].

Figure 1 shows the radial electric field profile formed

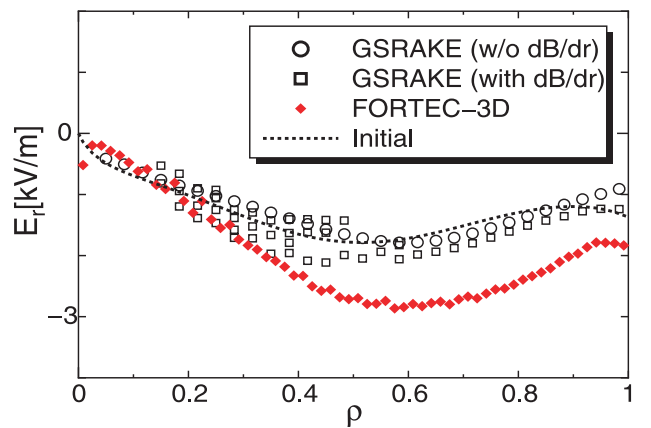


Fig. 1 Ambipolar electric field profile in the case $B_0 = 1.65$ T, $R_{ax} = 3.7$ m, and $T_e = T_i = 1.0$ keV on the magnetic axis. The horizontal axis is the normalized minor radius $\rho = \sqrt{\psi/\psi_{edge}}$. Diamond marks are the simulation result of FORTEC-3D, and circles and squares are estimations from GSRAKE. The dashed line is the initial E_r profile given in FORTEC-3D.

at a quasi-steady state at $t = 0.5\tau_i$, where τ_i is evaluated at $\rho = 0.5$. In this figure, the estimation of the ambipolar E_r profile is predicted by solving Γ_i as well as Γ_e from GSRAKE to seek the root that satisfies $\Gamma_e(E_r) = \Gamma_i(E_r)$ on each radial position. We show here two estimations from GSRAKE by turning on/off the contribution of the $\partial B/\partial\rho$ term in the ripple-averaged kinetic equation. This term is related to the poloidal component of ∇B drift motion. Γ_i obtained from GSRAKE shows a somewhat oscillatory behavior on the change of E_r if the $\partial B/\partial\rho$ term is included, while Γ_e is not significantly affected by this term. Therefore, we show in Fig. 1 some candidates of the solution for the ambipolar E_r obtained from GSRAKE calculated with the $\partial B/\partial\rho$ term. Neglecting this term makes the estimated ambipolar- $|E_r|$ value slightly smaller as can be seen in Fig. 1. In both cases, it is predicted that there is only a negative root (ion root) in the entire region, and the result of FORTEC-3D is also settled in a negative E_r profile. In the outer-half of the plasma $\rho > 0.5$, the ambipolar E_r value from FORTEC-3D and from GSRAKE differs by as much as 50%. This difference is apparently due to the fact that the ripple-averaged kinetic equation neglects these physics which are contained in the δf formulation, such as the FOW effect, rigorous treatments of collision term, and exact drift motion without averaging over a bounce time. Among them, we expect that the major factor leading to the difference in E_r is the FOW effect, especially for a low-collisionality plasma. Further inspection is described later. On the contrary, as shown in Fig. 2, the ambipolar flux obtained by FORTEC-3D shows close agreement with the predictions by GSRAKE in the case both with and without- the $\partial B/\partial\rho$ term to make the $\Gamma_{i,e}$ -tables. Since Γ_i generally has a steep peak on the negative side close to $E_r = 0$ as illustrated in Fig. 3, it is expected that a small difference of Γ_i between FORTEC-3D and GSRAKE due to the non-local effect would change the ambipolar condition if the root is close to the peak position. In Fig. 3, one can also see that ambipolar flux changes only slightly on the change of the ambipolar E_r because Γ_e is insensitive to the change of E_r compared with Γ_i .

The non-local effects on ion transport considered by FORTEC-3D can be classified into two types. The first type is the finiteness of the radial drift widths of helically and toroidally trapped orbits. In tokamaks, trapped particles sometimes have an orbit width as large as several tens % of the minor radius, and we have shown that neoclassical heat flux and the ambipolar condition in tokamaks are affected by the FOW effect of the large potato orbits appearing in the core region of tokamaks [17, 18]. In the helical LHD configuration, however, the orbit width of helically trapped particles is small and its FOW effect is expected to be weak. A stronger effect on neoclassical transport in LHD will arise from the FOW effect of transit orbits, which show a transition between helically and toroidally trapped (or passing) orbits. If the collisionality is small, some ion particles can drift a long distance in the radial direction by

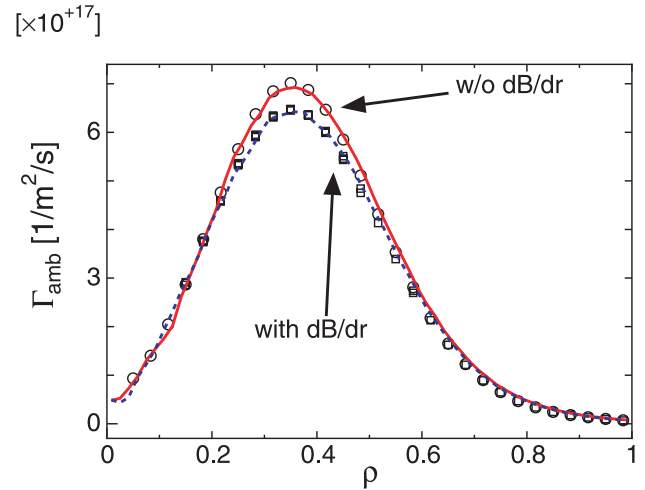


Fig. 2 Comparison of the ambipolar particle flux between GSRAKE (circles and squares) and FORTEC-3D simulations (solid and dashed lines). The circles and solid lines are results by using $\Gamma_{i,e}$ -tables of GSRAKE neglecting the $\partial B/\partial\rho$ term, while this term is included in the results plotted by squares and dashed lines.

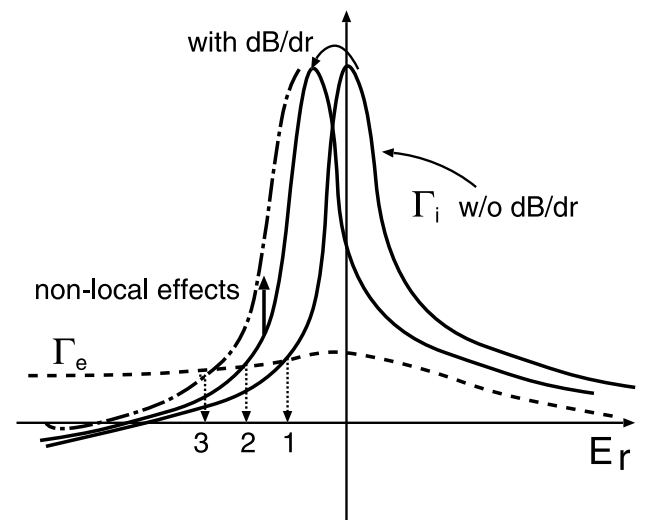


Fig. 3 Illustration of particle fluxes Γ_i and Γ_e seen as functions of E_r . By including the $\partial B/\partial r$ term (poloidal component of ∇B drift) and non-local effects, ambipolar E_r changes $1 \rightarrow 2 \rightarrow 3$ according to the change in Γ_i .

transitions. The second type is the direct orbit loss at the plasma boundary. In FORTEC-3D, this effect is included by killing the simulation markers which escape from the LCFS. Since we neglect the precise loss mechanisms of bulk ions by collisions between neutrals or impurities, and the real orbit in a stochastic magnetic field at the peripheral region are not included, our simulation is regarded as a simple model of orbit loss by a virtual limiter placed close to the LCFS.

In order to investigate these non-local effects on the formation of an ambipolar electric field, we carried out

two simulations: (a) by increasing the strength of magnetic field 4-times (though it is not achievable in real LHD experiment) that of the case shown in Fig. 1, and (b) by changing the magnetic axis position to $R_{ax} = 3.6$ m. In both simulations, n and T profiles are the same as in the previous case. Before explaining the simulation result, we mention here the collisionality in these simulations. The collisional regime of helical plasma is usually classified by the normalized factor $\nu_h^* \equiv qR_0 v_i / v_{th} \epsilon_h^{3/2}$ for a single-helicity case, where $\nu_i = \tau_i^{-1}$ and $\epsilon_h = B_{l,m}/B_0$ describes the relative magnitude of the Fourier component of the helical field. Though there is a proper definition for ϵ_h for a multi-helicity case [16], we use an approximation, in which $\epsilon_h \approx B_{2,10}/B_0$ as $B_{2,10}$ is the major helical component for a LHD configuration. The other two parameters used here to distinguish the plasma collisionality are $\nu_{eff} \equiv \nu_i/\epsilon_h$ and $\omega_E = |E_r|/rB_0$, which represent the effective collisionality for ripple-trapped particles and the $E \times B$ rotational frequency, respectively. In the simulation shown here, for example at $\rho = 0.7$ in the $R_{ax} = 3.7$ case, these parameters are $\epsilon_h = 0.12$, $\nu_h^* = 0.36$, $\nu_{eff} = 3.9 \times 10^3$, and $\omega_E = 4.0 \times 10^3$. These parameters are almost the same in the $R_{ax} = 3.6$ case shown below. Since $\nu_h^* \ll 1$, the plasma is well within the $1/\nu$ regime. Moreover, $\omega_E \approx \nu_{eff}$ means that the collisional regime is around the transition layer from the $1/\nu$ regime to $\nu^{1/2}$ regime, where the collisionless transition between trapped and untrapped orbits as well as the collisional diffusion of ripple-trapped particles contributes to the radial transport. In this collisionality, the radial transport level strongly depends on E_r (diffusion coefficient $D \sim 1/\nu$ in the $1/\nu$ regime and $\sim \nu^{1/2}/E_r^{3/2}$ in the $\nu^{1/2}$ regime [16]), and the finiteness of the transition particle orbit is expected to have an effect on the particle transport.

Now let us examine the simulation results in Figs. 4 and 5. In the strong B-field case, the discrepancy in the ambipolar E_r between GSRAKE and FORTEC-3D is small in the edge region $\rho > 0.8$, while a clear difference remains in the core region $0.2 < \rho < 0.8$. If the magnetic axis is shifted to $R_{ax} = 3.6$ m, one can see that the discrepancy in the ambipolar E_r becomes smaller than that in the case $R_{ax} = 3.7$ m. It is known that in LHD plasma, the neoclassical transport level is suppressed by shifting the magnetic axis inward [19]. In view of single particle orbit, this improvement of plasma confinement results from the fact that the radial excursion of transit orbit in an inwardly shifted configuration is shrunk as the Fourier components of the magnetic field spectrum change toward a “ σ -optimized” field [20]. Therefore, the non-local effect brought by transit particles, which is correctly evaluated in the δf simulation, is expected to have less effect on the total neoclassical transport in the case of $R_{ax} = 3.6$ m, and then the ambipolar E_r obtained from FORTEC-3D is close to the result obtained by GSRAKE, which is a small-orbit-width transport model. On the other hand, improvement in the confinement of transit orbit is not expected by changing only the abso-

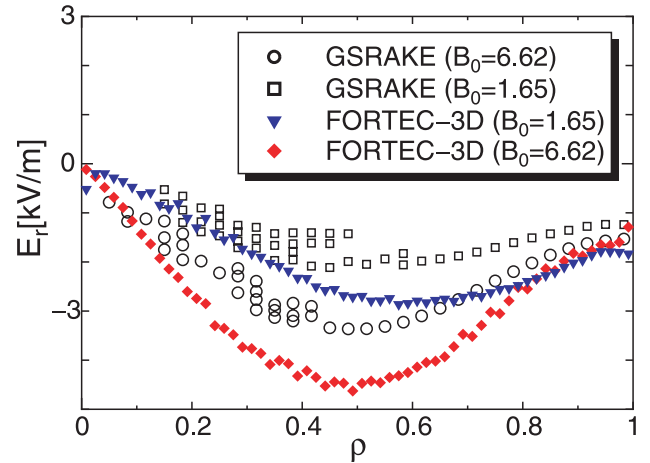


Fig. 4 Comparison of the ambipolar electric field in different strength of the magnetic field. Open circles and squares are the predictions from GSRAKE, and diamond and triangle marks are the results of FORTEC-3D at $t = 0.5\tau_i$.

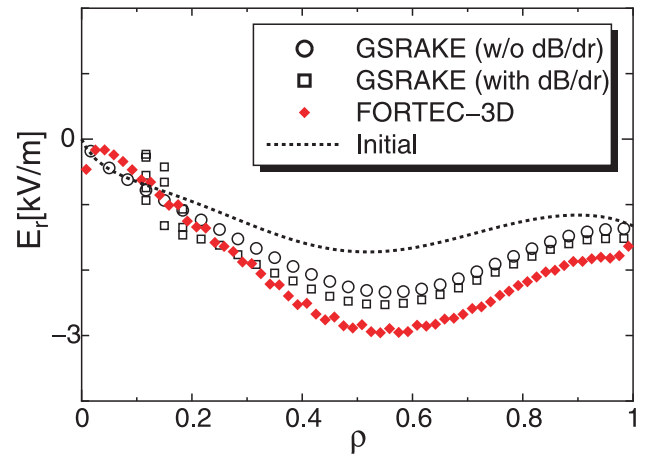


Fig. 5 Ambipolar electric field profile in an inward-shift configuration ($R_{ax} = 3.6$ m).

lute strength of the magnetic field. Note here that, since the plasma pressure is very low ($\beta \sim 0.01\%$) in the simulations we show here, the relative magnitude of each Fourier component of magnetic field is almost fixed on the change of absolute strength of it. From the result shown in Fig. 4, it is considered that the orbit-loss transport at the edge region is suppressed because the strong magnetic field shrinks the orbit width of toroidally trapped particles, and the difference of ambipolar E_r between GSRAKE and FORTEC-3D becomes smaller in the strong B-field case. The discrepancy of the ambipolar E_r between $0.2 < \rho < 0.8$ seems larger for the strong magnetic field case shown in Fig. 4. Note here that the $E \times B$ drift, which reduces the radial particle drift and transport in the collisionless regime, is proportional to E_r/B . From the result of FORTEC-3D simulation shown in Fig. 4, the fraction in the weak and strong B-field cases at $\rho = 0.5$ are $E_r/B = 1.7$ and 0.71 , respec-

tively. This suggests that the ion flux is suppressed enough to satisfy the ambipolar condition by a weaker $E \times B$ velocity in the stronger magnetic field case, that is, in the smaller orbit width case. Therefore, the apparent large discrepancy of E_r does not contradict our assertion that the FOW effect and its suppression by the $E \times B$ drift are the important factors in determining the ambipolar electric field. In conclusion, it is found that the non-local effects of loss cone particles and transit particles are important for a quantitatively reliable evaluation of the ambipolar electric field.

Next, we carried out a simulation in which the electron temperature is set 1.5 times larger than in the first case. The $\Gamma_e(\rho, E_r)$ -table constructed from GSRAKE is shown in Fig. 6. It has a peak around $E_r \approx 0$, which is a typical tendency of neoclassical flux in the $1/\nu$ regime. The ambipolar condition predicted by GSRAKE is plotted in Fig. 7. Note here that the $\partial B/\partial \rho$ term is dropped in this case in order to avoid numerical ambiguity in determining the ambipolar roots by GSRAKE, as shown in Fig. 1. It is predicted that triple roots exist in the range $0.2 < \rho < 0.5$. The middle root is an unstable root, thus the E_r profile will be settled in either a positive or a negative root. The simulation result of the δf simulation is also shown in Fig. 7. One can see close agreement of the resulting E_r profile between GSRAKE and FORTEC-3D regarding the radial position where positive and negative roots appear. It takes $2.5\tau_i$ to reach the quasi-steady state plotted in this figure, which is much longer than the previous cases in which only an ion root is expected. The large negative root at the edge is formed by the orbit loss of ions. It has evolved deeper than that seen in Fig. 1 because the simulation time is longer. It is worth noting that the edge E_r value in the simulation reached the steady state at $t \approx 2\tau_i$ and the strong $E \times B$ rotation at the edge region prevented simulation markers from leaking out of the plasma.

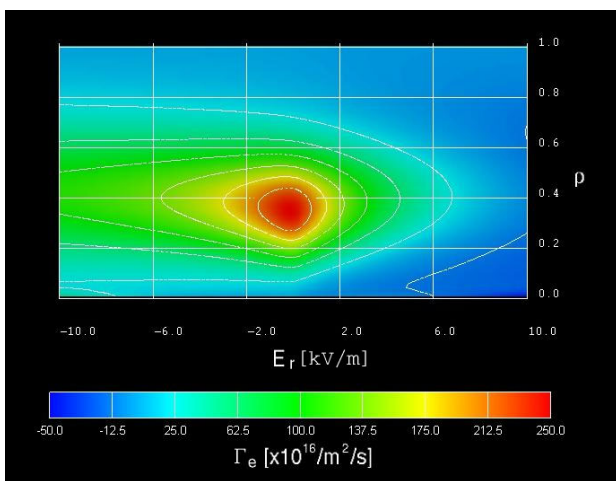


Fig. 6 Contour-plot of Γ_e -table calculated by GSRAKE in the case $T_e = 1.5, T_i = 1.0$ keV on the magnetic axis. It has a peak at $\rho \approx 0.35, E_r \approx -1.0$ keV.

The ion root E_r seen in $\rho > 0.6$ has a discrepancy between the results obtained by GSRAKE and FORTEC-3D as it is seen in Fig. 1. This can be attributed to the non-local effects and to the smallness of the ambipolar $|E_r|$ of GSRAKE estimation without the $\partial B/\partial \rho$ term. On the other hand, the positive root (electron root) shows close agreement between these two numerical codes. Generally, neoclassical flux is suppressed in an electron root compared with that in an ion root. This tendency can also be seen in Fig. 9 mentioned later, which shows the change in I_i before and after the transition from the ion to the electron root. The suppression of I_i in the positive electric field means that the typical radial drift width is also suppressed in the presence of positive- E_r . Therefore, the non-local effect on neoclassical flux in the δf code is expected to be smaller in the electron root, and accordingly the resultant ambipolar field profiles obtained by GSRAKE and by FORTEC-3D become closer. In the middle layer $0.4 < \rho < 0.6$, the electric field profile obtained by FORTEC-3D shows an oscillatory behavior. Bifurcation of the ambipolar condition occurs in this layer, and we think this oscillation is due to a numerical instability of FORTEC-3D at the discontinuous layer of the radial electric field in the time evolution of E_r according to eq. (3). A more suitable numerical method for the evolution of the E_r field, which may have discontinuous points in the radial direction as shown in Fig. 7, should be adopted in the future.

The time development of E_r and I_i on the flux surfaces $\rho = 0.30, 0.35$, and 0.40 are plotted in Figs. 8 and 9, respectively. Note that the time evolution of the radial electric field as well as that of weight w are stopped arti-

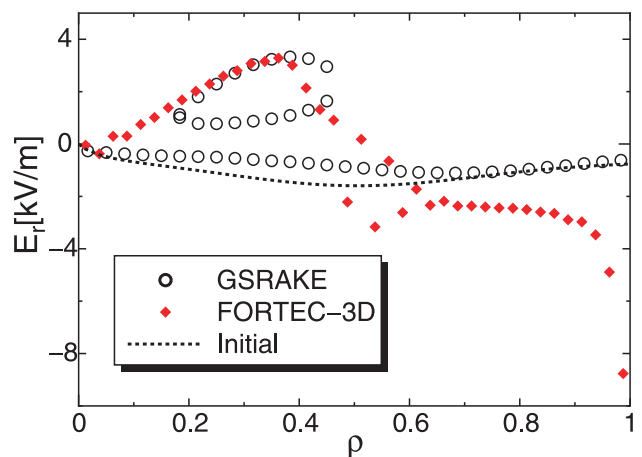


Fig. 7 Ambipolar electric field profile simulated by using the Γ_e -table in Fig. 6 when it reaches a quasi-steady state at $t = 2.5\tau_i$. Between the region $0.2 < \rho < 0.5$, multiple roots for ambipolar condition $\Gamma_e = I_i$ is expected from GSRAKE, and the result of FORTEC-3D shows a bifurcation from negative to positive root in that region. A strong negative E_r at the edge region is formed as a result of the ion orbit-loss occurred there.

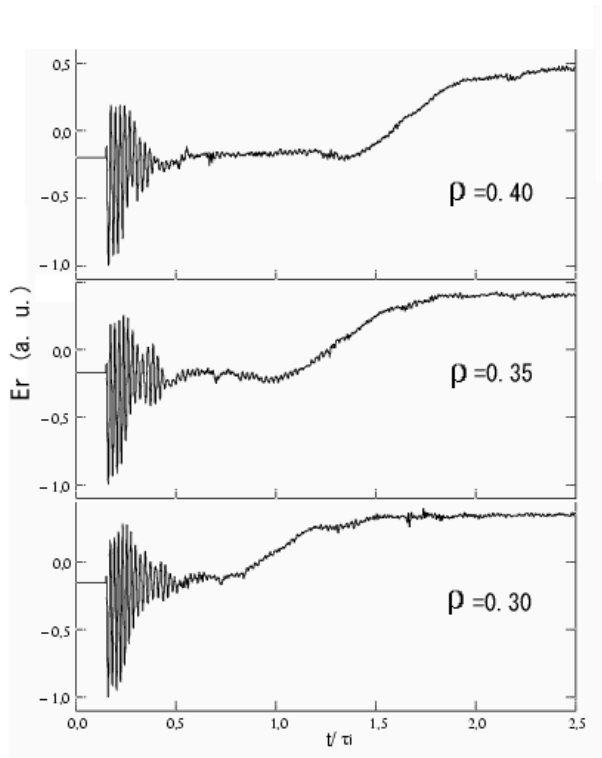


Fig. 8 Time evolution of the radial electric field on the flux surfaces $\rho = 0.30, 0.35,$ and 0.40 in the same case as in Fig. 7. The horizontal axis is the simulation time normalized by $\tau_i(\rho = 0.5)$.

cially in the initial phase until $t = 0.2\tau_i$ in order to avoid an excessively large spike at the onset of the oscillation of E_r and Γ_i . On these surfaces, the radial electric field oscillates rapidly around the negative root in the beginning phase. By taking the power spectrum, the oscillation is identified as the geodesic acoustic mode as shown in Fig. 10, of which frequency is estimated as $\omega_{\text{GAM}} = \sqrt{7}v_{\text{th}}/2R_0$ [2] based on neoclassical transport analysis in a simple circular-cross section tokamak case, where v_{th} is the ion thermal velocity on each flux surface. The GAM oscillation damps and the E_r on each surface settles in the negative root. Then, a transition of E_r happens on $\rho = 0.30$ at $t = 0.8\tau_i$ and the transition propagates to the outer surfaces as seen in Fig. 8. Since our δf code treats the evolution of plasma as an initial value problem containing no source terms, the final steady E_r profile depends on the initial settings of the plasma state. Therefore, there is also the possibility of a steady ion root in some initial condition or by introducing source/sink terms to the simulation. Unlike in a local transport analysis such as GSRAKE which solves the ambipolar condition independently on each single flux surface, evolution of the ambipolar E_r profile in a global simulation is determined by the total balance of particle and momentum transport in the whole plasma region. Though the details of the triggering mechanism are still unclear because we have examined only one case, the simulation result shows

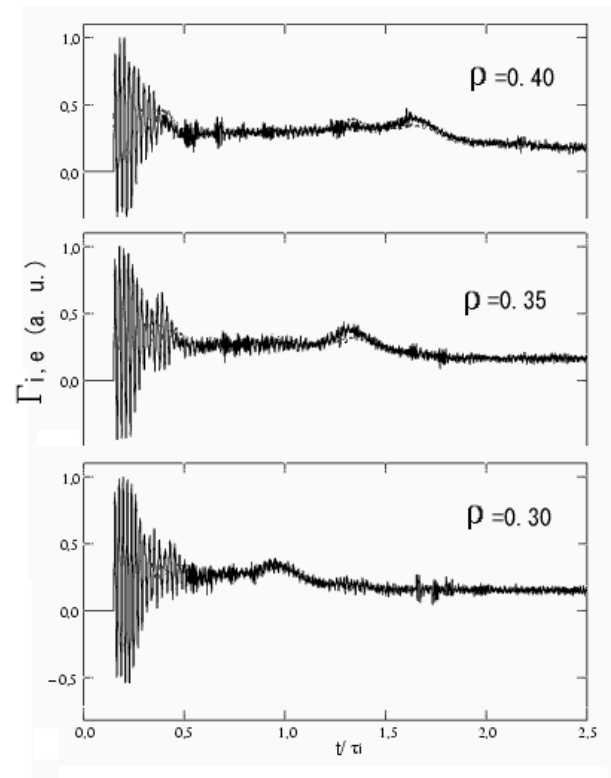


Fig. 9 Time evolution of the radial particle fluxes on the flux surfaces $\rho = 0.30, 0.35,$ and 0.40 in the same case as in Fig. 7. Solid line is the ion particle flux Γ_i and dashed line is Γ_e (almost hidden by the solid line).

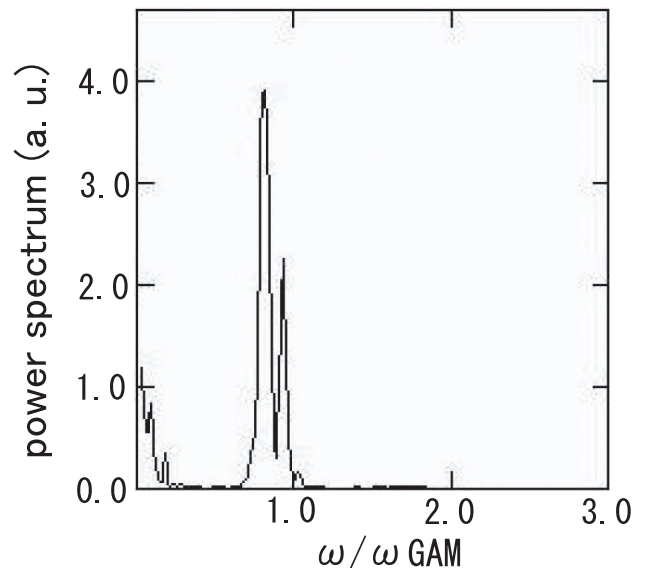


Fig. 10 The power spectrum of E_r oscillation taken in the time span $0.2 < t/\tau_i < 0.5$ on $\rho = 0.35$ surface shown in Fig. 8. The theoretical value of GAM frequency is given by $\omega_{\text{GAM}} = \sqrt{7}v_{\text{th}}/2R_0$.

that the transition and formation of the ambipolar electric field contain a non-local nature.

4. Summary

We have developed a neoclassical transport simulation code FORTEC-3D to investigate non-local and time-dependent phenomena in neoclassical transport in non-axisymmetric systems such as LHD. It has been shown in this paper that our hybrid simulation model designed to solve ion and electron fluxes worked successfully and that non-local neoclassical transport affects the magnitude of the ambipolar electric field. The existence of a non-local transition mechanism has also been shown. Therefore, we consider the use of the global transport simulation model as introduced here to be important in the investigation of transport phenomena in the short time scale such as the formation and transition of the ambipolar electric field in non-axisymmetric systems. We will continue to develop the δf code in order to stabilize the time evolution of E_r at the point where the E_r profile changes from a positive to a negative root, and plan to investigate the above issues based on detailed simulations using FORTEC-3D.

As shown in Fig. 7, a strong negative E_r is formed at the edge region. This is due to the orbit loss of ions at the LCFS. The killing and recycling processes for the markers adopted here are artificial ones and do not reflect the physical processes in the plasma's edge region such as charge exchange and re-entering of ions. Introducing such physical mechanisms will make it possible to simulate the formation of the edge transport barrier. To introduce a physical source or a sink term, the procedure of marker recycling explained in Sec. 2 can be extended by adding a source term in the lhs of eq. (7). The improvement of the simulation model by adding the source and sink terms will make it possible to apply the simulation to various studies concerning neoclassical transport phenomena and to compare the results with experimental data.

Acknowledgements

One of the authors (S.S.) would like to thank Prof. C.D. Beidler of the Max-Planck Institute for Plasma Physics, Garching for offering us the GSRAKE code. This work is performed under the auspices of the NIFS Collaborative Research Program, Nos. NIFS05KDAD004 and NIFS05KNXN040.

- [1] S.V. Novakovskii *et al.*, Phys. Plasmas **4**, 4272 (1997).
- [2] M. Okamoto *et al.*, J. Plasma Fusion Res. **78**, 1344 (2002).
- [3] W.X. Wang *et al.*, Plasma Phys. Control. Fusion **41**, 1091 (1999).
- [4] S. Brunner *et al.*, Phys. Plasmas **6**, 4504 (1999).
- [5] K.C. Shaing and R.D. Hazeltine, Phys. Fluids B **4**, 2547 (1992).
- [6] D.E. Hastings *et al.*, Nucl. Fusion **25**, 445 (1985).
- [7] K.C. Shaing and J.D. Callen, Phys. Fluids **26**, 3315 (1983).
- [8] L.M. Kovrizhnykh, Nucl. Fusion **24**, 851 (1984).
- [9] S. Toda and K. Itoh, Plasma Phys. Control. Fusion **46**, 1039 (2004).
- [10] C.D. Beidler *et al.*, Plasma Phys. Control. Fusion **37**, 463 (1995).

- [11] C.D. Beidler and H. Maaßberg, Plasma Phys. Control. Fusion **43**, 1131 (2001).
- [12] A. Iiyoshi *et al.*, Fusion Technol. **17**, 169 (1990).
- [13] A.H. Boozer, Phys. Fluids **23**, 904 (1980).
- [14] S.P. Hirshman and O. Betancourt, J. Comput. Phys. **96** 99 (1991).
- [15] S. Satake *et al.*, NIFS Report NIFS-828 (2005).
- [16] M. Wakatani, *Stellarator and Heliotron devices* (Oxford Univ. Press, New York, 1998), p. 291.
- [17] S. Satake, M. Okamoto and H. Sugama, Phys. Plasmas **9**, 3946 (2002).
- [18] S. Satake and M. Okamoto, J. Plasma Fusion Res. SERIES **6**, 144 (2004).
- [19] S. Murakami *et al.*, Nucl. Fusion **42**, L19 (2002).
- [20] H.E. Mynick, T.K. Chu and A.H. Boozer, Phys. Rev. Lett. **48**, 322 (1982).